ARMY RESEARCH LABORATORY

Modeling Thermal Ignition of Energetic Materials

by Norman J. Gerri and Ellen Berning

ARL-TR-3369 **November 2004**

NOTICES

Disclaimers

The findings in this report are not to be construed as an official Department of the Army position unless so designated by other authorized documents.

Citation of manufacturer's or trade names does not constitute an official endorsement or approval of the use thereof.

Destroy this report when it is no longer needed. Do not return it to the originator.

Army Research Laboratory
Aberdeen Proving Ground, MD 21005-5068

ARL-TR-3369 **November 2004**

Modeling Thermal Ignition of Energetic Materials

Norman J. Gerri and Ellen Berning
Survivability/Lethality Analysis Directorate, ARL

REPORT DOCUMENTATION PAGE

Form Approved
OMB No. 0704-0188

1. REPORT DATE *(DD-MM-YYYY)*	2. REPORT TYPE	3. DATES COVERED (From - To)
November 2004	Final	October 2003–October 2004

4. TITLE AND SUBTITLE
Modeling Thermal Ignition of Energetic Materials

5a. CONTRACT NUMBER

5b. GRANT NUMBER

5c. PROGRAM ELEMENT NUMBER

6. AUTHOR(S)
Norman J. Gerri and Ellen Berning

5d. PROJECT NUMBER
D6-75

5e. TASK NUMBER

5f. WORK UNIT NUMBER

7. PERFORMING ORGANIZATION NAME(S) AND ADDRESS(ES)
US Army Research Laboratory
AMSRD-ARL-SL-BE
Aberdeen Proving Ground, MD 21005-5068

8. PERFORMING ORGANIZATION REPORT NUMBER
ARL-TR-3369

9. SPONSORING/MONITORING AGENCY NAME(S) AND ADDRESS(ES)

10. SPONSOR/MONITOR'S ACRONYM(S)

11. SPONSOR/MONITOR'S REPORT NUMBER(S)

12. DISTRIBUTION/AVAILABILITY STATEMENT
Approved for public release; distribution is unlimited.

13. SUPPLEMENTARY NOTES

14. ABSTRACT
This report documents an attempt to computationally simulate the mechanics and thermal regimes created when a threat perforates an armor envelope and comes in contact with stowed energetic material (M30 granular propellant). Fragment simulating penetrators (FSP) of 208 and 830 gr were fired into plates of AISI 4340 steel hardened to a Rockwell C = 40. The exiting fragments were captured in a polymeric material with a melting point equivalent to the ignition temperature of the propellant. Paralleling the field experiment, a series of CTH 3D finite element runs were carried out using the same initial conditions as the experiments. The temperatures calculated by the CTH codes are compared to the experimental value. Experimental shots fired into live propellant at velocities selected from the CTH runs gave ignition or no ignition as predicted within reasonable limits.

15. SUBJECT TERMS
CTH, penetration mechanics, M30 propellant ignition, finite element, finite element mechanical and thermal simulation, fragment temperature measurements

16. SECURITY CLASSIFICATION OF:			17. LIMITATION OF ABSTRACT	18. NUMBER OF PAGES	19a. NAME OF RESPONSIBLE PERSON
a. REPORT	b. ABSTRACT	c. THIS PAGE			Norman J. Gerri
UNCLASSIFIED	UNCLASSIFIED	UNCLASSIFIED	UL	26	19b. TELEPHONE NUMBER (*Include area code*) 410-278-6327

Standard Form 298 (Rev. 8/98)
Prescribed by ANSI Std. Z39.18

Contents

List of Figures

List of Tables

Acknowledgments

The authors would like to thank Jonathan Montgomery, Weapons and Materials Research Directorate (WMRD), for his most valuable assistance and willingness to share his expertise in the behavior of metals; Dr. Patrick Baker, WMRD, for his advice and insight; and Dr. Larry Vanderkief (contractor), WMRD, for his meticulous hot fragment conductive ignition experiments.

The authors would also like to thank Rick Kane, Survivability/Lethality Analysis Directorate (SLAD), and Mark Ward, SLAD, for the near-perfect indoor range fragment experiments and Danny Dominick, SLAD, Jim Poole, SLAD, and Maurice Clark (contractor), SLAD, for the live propellant target assembly and precise gunnery.

INTENTIONALLY LEFT BLANK.

1. Introduction

The current emphasis on fast, maneuverable, lightly armored vehicles has lowered the basic threat-level protection from large-caliber artillery rounds, shaped charges and kinetic energy (KE) penetrators to lesser threats represented by small-caliber penetrators and artillery-generated fragments. Beside the mechanical damage expected from perforating threats, there is now the added consideration of multiple thermal sources in close proximity to energetic materials such as propellants, explosives, and fuel. In addition, power cables, sensors, and other thermally sensitive materials are at risk. As primary armor protection decreases, secondary protection offered by storage compartments and component casings becomes an essential survivability factor.

2. Objectives

The objective of this study is to devise a computational methodology to predict the thermal regimes which can lead to the ignition of stowed propellants and other energetic materials in close contact with armor-perforating threats. Secondary objectives are estimates of the residual penetrators' mass, velocity, and geometry for collateral damage predictions.

3. Approach

Using the FATEPEN penetration equations (*1*), estimate the impact velocity for each penetrator mass/ target thickness combination that will yield an exit or residual velocity of ~300–400 m/s.

Transferring these initial conditions to the experimental range and firing into simulated inert propellant, adjust the impact velocities to obtain a range of exit velocities that will permit the residual penetrators to be captured in a live propellant bed.

Substitute these initial conditions into the CTH shock physics code (*2*) and simulate the perforation mechanism and residual penetrator characteristics for 100–200 μs. Duplicate the CTH runs on the experimental range and compare results.

4. Experimental Ballistic Results

4.1 Materials

To avoid ambiguity in material properties, the American Iron and Steel Institute (AISI) 4340 steel plate (manufactured to AMS 6359 specifications and tempered to Rockwell C = 39–40) was selected for the target plate. Target plates were obtained in nominal thicknesses of 6.35, 9.53, and 12.7 mm. Heat treatment and scale removal reduced these thicknesses by 0.76 mm. The selected ballistic threats were 208-gr (0.50-cal.) and 830-gr (20-mm) right circular cylinder fragment-simulating projectiles (FSPs) with a length-to-diameter (L/D) ratio = 1 and machined from the AISI 4340 25.4-mm rod and tempered to Rockwell C = 29–30. The energetic material was M30A1 propellant downloaded from XM 232 155-mm modular artillery charges (MACs).

4.2 Ballistic Apparatus

The ballistic measurements were conducted using the experimental test setup shown in figure 1. The preselected experimental parameters included the mass, geometry, and velocity of the impacting FSP and the thickness of the target plate. Measurements were of the mass, temperature, and velocity of the exiting or residual FSP and the associated plug from the target plate.

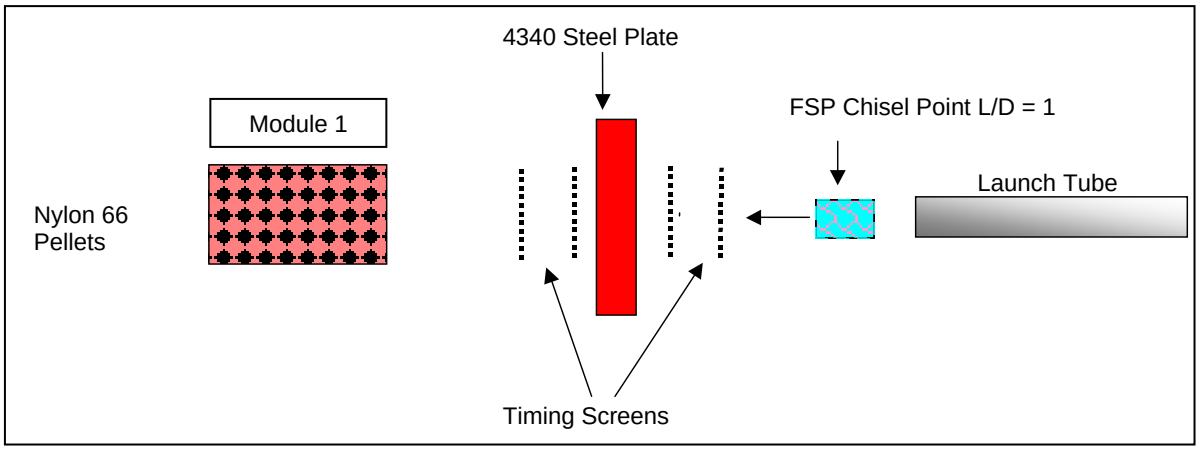

Figure 1. Ballistic test schematic.

The modular recovery system was designed to capture the residual FSPs without damage or distortion and, at the same time, measure the temperature of the FSP as it comes to rest. All shots were fired at 0° obliquity, and impact velocities were selected by FATEPEN (*1*) to give residual velocities in the range of ~1000 ft/s to facilitate capture of the residual FSP and plug sheared from the wall of the target plate.

4.3 Ballistic Results

The ballistic results for the 830- and 208-gr FSPs are given in table 1.

Table 1. Comparison of 830- and 208-gr FSP CTH and experimental results.

Shot No.	Target (mm)	FSP (gr)	Experimental				CTH	
			Vimp (m/s)	Vres (m/s)	FSP RES (gr)	Plug (gr)	Vimp (m/s)	Vres (m/s)
1	5.59	830	620	431	768	135	609	303
2	5.59	830	623	476	770	167	—	—
3	5.59	830	631	482	767	180	—	—
4	8.76	830	712	415	717	343	701	239
5	8.76	830	712	411	733	330	—	—
6	8.76	830	714	413	737	346	—	—
7	11.9	830	736	303	694	465	732	151
8	11.9	830	735	322	682	462	—	—
9	11.9	830	734	283	695	464	—	—
10	5.59	208	806	473	183	75	793	303
11	5.59	208	801	466	183	76	—	—
12	8.76	208	758	276	162	152	732	NE
13	8.76	208	790	NE	—	133[a]	—	—
14	8.76	208	760	NE	—	131[b]	—	—

Notes: NE = no exit; Vimp = impact velocity; and Vres = residual velocity.
[a]Exit velocity of the plug = 247 m/s.
[b]Exit velocity of the plug = 209 m/s.

4.4 Propellant Ignition Limits

Propellant ignition temperatures are determined in the apparatus shown in figure 2.

An FSP was suspended in a vertical tubular furnace at a preset temperature until thermal equilibrium was obtained. The FSP was dropped into a small amount of propellant and the time to ignition noted. If ignition did not occur, the furnace temperature was raised and the experiment repeated (*3*). At FSP temperatures close to the ignition limit, the delay to ignition increased dramatically.

4.5 Hot Fragment Conductive Ignition (HFCI) Test Results

For the 830-gr FSP, the longest ignition delay was 18 s, indicating a very close proximity to the ignition limit. Several runs were carried out in the vicinity of the lowest ignition temperature to establish a statistical go/no-go confidence level. The experimental results for the 830-gr FSP indicated an ignition temperature of 249.8 ± 5 °C, as determined from the experimental results shown in figure 3. Similar experiments with the 208-gr FSP gave an ignition temperature of 256.1 ±6 °C. Runs 4 and 14 used ground propellant instead of the granular form, without any noticeable effect.*

*The nominal size of the M30A1 propellant grain is 25.4 × 12.7 mm.

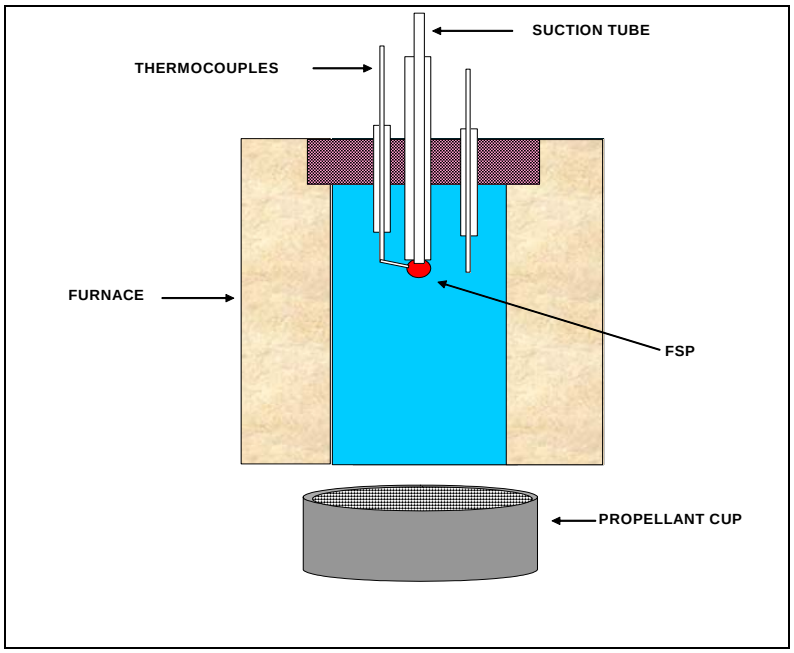

Figure 2. Hot fragment conductive ignition apparatus.

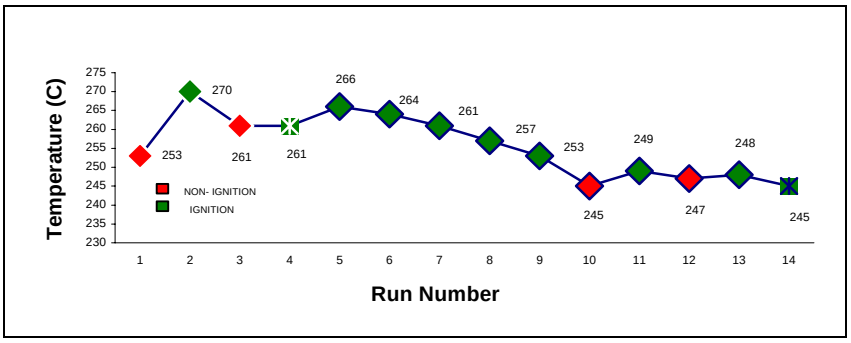

Figure 3. HFCI experimental results for the 830-gr FSP.

4.6 Residual Temperature Measurements

Infrared (IR) Techniques: Residual FSP temperature measurements proved to be a significant challenge. Originally, it was anticipated that high-speed IR camera measurements would thermally characterize the residual FSP just prior to contact with the propellant. Because of emissivity factors and the limited vertical field of view of 75 mm for residual penetrators at ~300 m/s, the IR camera technique was not satisfactory. A two-color IR technique which reduces emissivity factors has been suggested as a possibility for future measurements.

4.6.1 Polymeric Melting Points

The most successful thermal indicators were polymeric materials with sharp melting points in the vicinity of the propellant ignition temperatures (module 1, figure 1). Using the MatWeb Material Properties website (*4*), a search for polymers to match the melting point, density, and thermal conductivity of the M30A1 yielded nylon 6 6 with 30% fiberglass filler as a suitable match (table 2). Note that nylon 6 6 is available in 6- × 12-mm pellets.

Table 2. Nylon propellant simulant properties.

	MP (°C)	**δ (g/cm^3)**	**λ (W/m-K)**
M30A1	250	1.62	0.42
nylon 6 6	249	1.62	0.55

Dropping a 830-gr FSP heated to 255 °C into a bed of nylon 6 6 pellets gave the results shown in figure 4. The numerous nylon pellets melted to the sides of the FSP indicated a sharp melting point and the possibility of ignition if live propellant had been used.

Figure 4. Nylon beads melted on residual FSP.

Unfortunately, single polymers could only indicate that fragment temperatures were either above or below the ignition limit. Experiments are in progress to combine colored polymeric materials with different melting points, which will provide a broad thermal profile for a residual FSP.

Figure 5 shows the degree of attachment of nylon 6 6 pellets to 208- and 830-gr FSPs as a function of FSP mass and impact velocities on 5.56- and 8.76-mm 4340 steel plates, respectively.

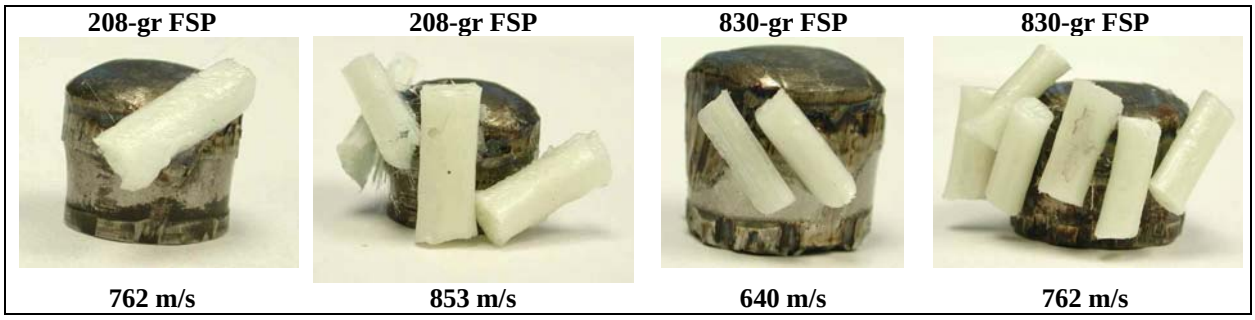

Figure 5. Experiments with FSPs nylon 6 6 at various impact velocities.

As expected, higher velocities give higher FSP temperatures as indicated by the number of pellets attached to each FSP mass. Subsequent range experiments, described in section 4.6.4, demonstrated that the higher velocities show above would have resulted in propellant ignition.

4.6.2 CTH Simulation Results

CTH, a shock physics code designed to model ballistic impact and penetration (*2*), was used to run a series of two-dimensional (2-D) simulations of the ballistic experiments described under the experimental ballistic results section.

Figure 6 shows the general configuration at time zero for all runs. The left side of the diagram represents the color-coded temperature regimes and the right side a color-coded material designation. In this case, since both the target and the projectile were of the same material, the target had been assigned a different color to avoid confusion. Each run was conducted in 2-D.

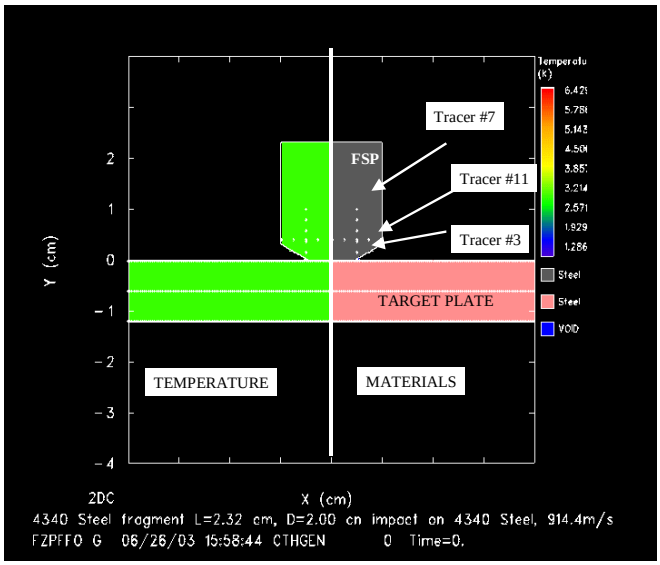

Figure 6. Simulation setup.

Each FSP was oriented at the origin, symmetrically around the y axis. Tracer points,* used in these simulations to track velocity and temperature, were also shown in the diagram. Tracer points 3, 7, and 11 were chosen as representative of areas of low, medium, and high temperature, respectively.

Different thicknesses of steel plate were modeled to match the three plate thicknesses used in the experiment. The cell size in the mesh was 0.4 × 0.4 mm throughout the area of interest. The axisymmetric nature of the problem was exploited in order to reduce computation time.

The SESAME tabular option for iron was chosen as the equation of state model, since it was the recommended model when temperature was an important variable as in this simulation (*5*). The Johnson-Cook strength model (*6*), as well as the Johnson-Cook fracture model (*7*), was also selected using the default parameters for 4340 steel, Rockwell C = 30 (Rockwell C = 39/40 parameters were not available).

4.6.3 Results of Ballistic Simulations

The results, shown in table 1, compare the experimental residual velocities with the values with respect to the residual FSP velocities and the thermal ignition criteria determined by the nylon pellets. A second set of experiments assessed whether a connection could be made between the temperature of the FSP predicted by modeling and ignition of the M30A1 propellant. Figure 7 shows a residual FSP fired into a nylon bed as compared to an equivalent simulation. Note that the location of the nylon pellets corresponds to the high-temperature yellow-orange (~300 °C) region of the simulated FSP.

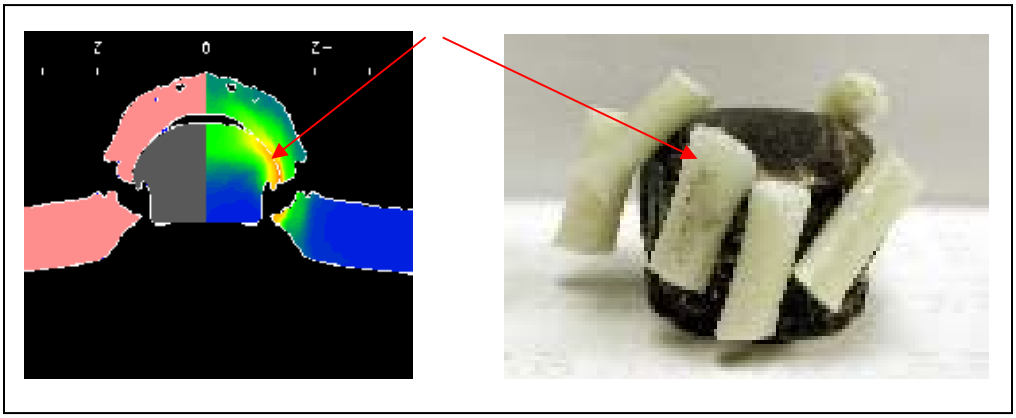

Figure 7. Comparison of CTH prediction and nylon experiment.

While the simulated results agreed, in general, with experimental results, the residual velocities were underpredicted, as shown in table 1. Qualitative agreement between the temperature distribution within the simulated FSP and experimental results is illustrated in figure 7. Areas of

*Lagrangian tracer points define a location in a material from which preselected data variables can be collected at regular time intervals in a history file.

the FSP to which the nylon 6 6 pellets adhered were consistent with model temperature predictions.

Model predictions are summarized in table 3 for both the 208- and 830-gr FSP. Experimentally, ignition occurred at impact velocities of 823 and 853 m/s for the 208-gr FSP and 707 m/s for the 830-gr FSP. Locations of tracer points 3, 7, and 11 were illustrated in figure 6.

Table 3. Comparison of simulations with experiment.

FSP (gr)	Impact Velocity (m/s)	Residual Velocity (m/s)	Fracture Option[a]	Tracer Pt. 7 Low Temp. (°C)	Tracer Pt. 3 Mid-Pt. Temp. (°C)	Tracer Pt. 11 High Temp. (°C)
208	762	146	p	105	206	350
208	793	232	p	118	208	372
208	808	245	p	122	209	384
208	823	275	p	125	211	392
208[b]	853	326	p	132	212	413
830	640	185	s	110	227	357
830[b]	707	276	s	116	233	383
830[b]	732	293	s	126	237	411
830[b]	762	330	s	133	242	431

[a]p = pressure option, and s = stress option.
[b]Experimentally indicated conditions under which propellant ignition should occur.

An important difference existed between the simulations conducted for the first (ballistic) and second (propellant ignition) set of experiments. In addition to the Johnson-Cook fracture model, another fracture model (*8*) was also used. This model determined fracture based either on stress or pressure. When fracture itself was of interest, the stress option was recommended. While using the "stress" option in the first set of simulations proved to be successful, an instability related to this option was discovered while running the second set of simulations. This instability expressed itself at impact velocities above ~765 m/s for the 208-gr FSP. Upon consultation with the CTH development team at Sandia National Laboratories (SNL), it was determined that this instability represented a problem with the code itself (the SNL team is working to resolve this issue). But in the meantime, these simulations were run using the "pressure" option. Runs utilizing the "pressure" option predicted slower residual velocities and slightly different temperatures than those using the "stress" option. (See table 4 for comparisons of the 208-gr FSP for "stress" vs. "pressure" options.) Figures 8 and 9 show side-by-side comparisons of CTH-generated simulations for 208-gr and 830-gr FSPs, respectively. These figures illustrate subtle differences in the simulated temperature distribution at varying impact velocities. The temperature distribution is shown at the left side of each FSP, with blue indicating the lowest temperature and red the highest.

Table 4. Simulated results for "stress" and "pressure" fracture options.

FSP (gr)	Impact Velocity (m/s)	Residual Velocity (m/s)	Fracture Option[a]	Tracer Pt. 7 Low Temp. (°C)	Tracer Pt. 3 Mid-Pt. Temp. (°C)	Tracer Pt. 11 High Temp. (°C)
208	762	146	p	105	206	350
208	762	225	s	103	204	363
830	701	189	p	126	228	380
830	701	276	s	116	233	383

[a]p = pressure option, and s = stress option.

From the modeling perspective, the most critical issue left to be resolved was experimental verification of temperatures predicted by the model. This verification was complicated by the fact that temperature was not uniform across the body of the FSP. While the "ignition–no ignition" threshold did provide a crude measure, a finer, more accurate measurement was crucial.

4.6.4 Propellant Ignition Experiments

The CTH simulation shown in figures 8 and 9 and the polymer shots in figure 5 indicate that at impact velocities above 800 m/s for the 208-gr FSP and above 700 m/s for the 830-gr FSP, ignition of live propellant should occur. To verify these predictions, model verification experiments were carried out in the apparatus shown in figure 10. Dense NOMEX felt pads were placed behind the target plate to catch any residual spall particles that may be generated.* High-density polypropylene pads were designed to slow down the projectile so that it came to a stop within the propellant bed. Inert propellant grains of the same size and density as M30A1 were used to determine the proper spacing. If ignition did not occur, the top of the box was removed to ensure the FSP stopped in the propellant bed.

The results, shown in table 5, were in excellent agreement with the predictions. It is interesting to note that shot 2 (ignition) and shot 4 (nonignition) had impact velocities just 4 m/s apart, indicating the sensitivity of the thermal source to impact velocity.

5. Conclusions

Range experiments show propellant response from no reaction to ignition within a 4-m/s spread in the impact velocity (table 5). These results demonstrate the importance of being able to simulate the vulnerability of our ammunition compartments to a variety of threats during the armored vehicle design process.

A computational model is developed using CTH for the purpose of simulating the impact conditions under which thermal ignition of energetic materials would occur upon perforation of an armor plate by fragments. While at this point results remain largely qualitative, they have

*No spall particles were detected in the NOMEX pads or in the propellant bed.

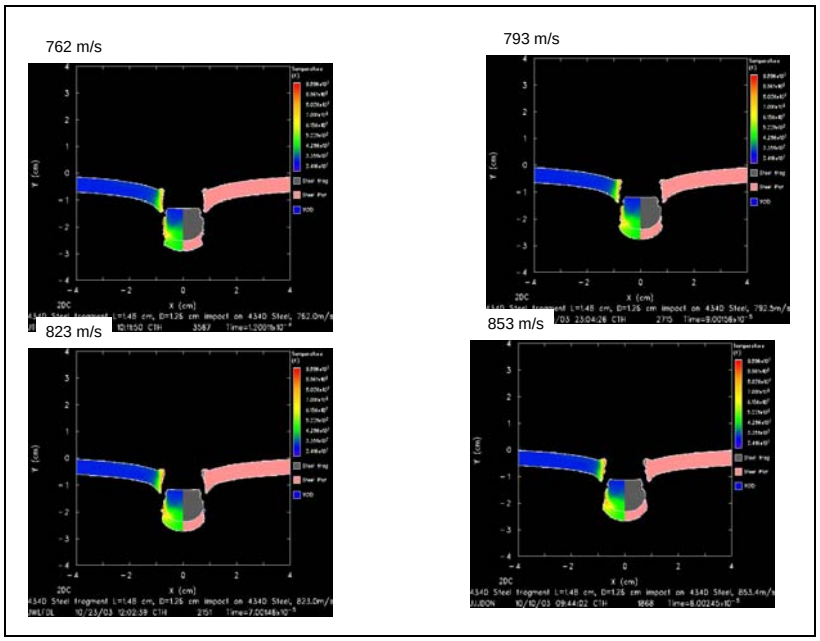

Figure 8. CTH simulations of 208-gr FSP at varying impact velocities.

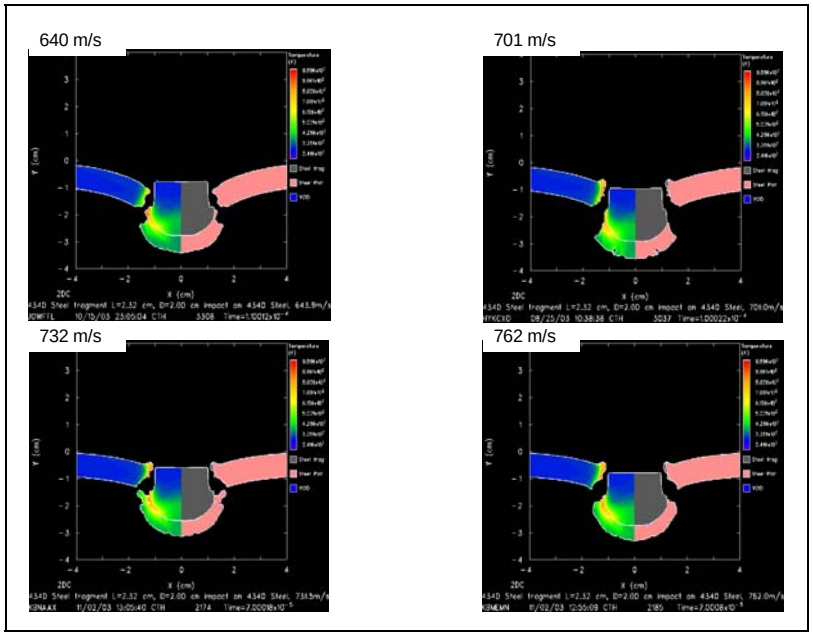

Figure 9. CTH simulations of 830-gr FSP at varying impact velocities.

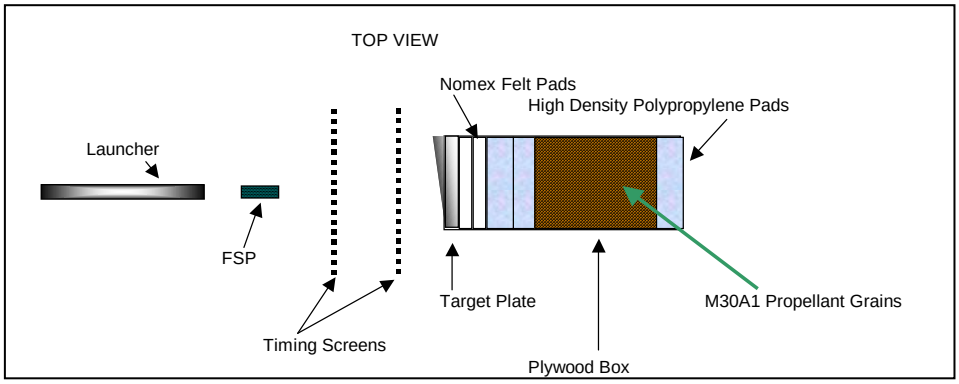

Figure 10. Propellant ignition experimental schematic.

Table 5. Propellant ignition verification results.

Shot No.	FSP Mass (gr)	Plate Diameter (mm)	Impact Velocity (m/s)	Ignition/ Nonignition	Ignition Time (s)
1	208	5.59	671	Nonignition	—
2	208	5.59	821	Ignition	12
3	208	5.59	754	Nonignition	—
4	208	5.59	817	Nonignition	—
5	208	5.59	848	Ignition	8
—	—	Limit	~819	—	—
6	830	8.76	644	Nonignition	—
7	830	8.76	614	Nonignition	—
8	830	8.76	669	Nonignition	—
9	830	8.76	707	Ignition	5
—	—	Limit	~687	—	—

been encouraging. The perforation mechanism appears to be adequately described and there is little doubt that the primary ignition site is the orange-yellow band that girdles the forward section of the residual fragment edge of the fragment (see the appendix). Among the outstanding issues are the discrepancies between the predicted exit velocities and experimental values. Also, the surprisingly sharp thermal gradients created by the work done in shearing off fragment material as it perforates the target plate raises the question of how to redefine the concept of an "ignition temperature" to a "thermal ignition profile" of the residual fragment. Subsequent experiments will attempt to define the relationship of the thermal ignition sites as a function of the impact velocity.

The current simulations will be rerun when all the necessary coefficients to the equation of state are available for 4340 Rockwell C = 40. In the future, we expect to join the CTH code to a heat transfer code and examine the competition between the rate of heat transferred to the propellant and the rate of heat transferred to the cooler parts of the FSP in the vicinity of the ignition limit.

6. References

1. Edquist, K. T., et al. *FATEPEN – Terminal Ballistic Penetration Model, Vol. 1*; Applied Research Associates: Littleton, CO, 2001.

2. McGlann, J. M.; Thompson, S. L; Elrick, M. G. CTH: A Three-Dimensional Shock Wave Physics Code. *International Journal of Impact Physics* **1990**, *10*, 351–360.

3. Law, H. C. The Hot Fragment Conductive Ignition Test. *18th JANNAF Combustion Meeting*, Jet Propulsion Laboratory, Pasadena, CA, 1981.

4. MatWeb Material Properties website. www.matweb.com (accessed July 2003).

5. Hertel, E. S., Jr.; Kerley, G. I. *CTH Reference Manual: The Equation of State Package*; SAND98-0947; Sandia National Laboratory: Albuquerque, NM, 1998.

6. Silling, S. A. *CTH Reference Manual: Viscoplastic Models*; SAND91-0292; Sandia National Laboratory: Albuquerque, NM, 1996.

7. Silling, S. A. *Use of Johnson-Cook Fracture Model in CTH*, CTH Reference Manual. Sandia National Laboratory: Albuquerque, NM, 1996.

8. McGlann, J. M. *CTH Reference Manual: Cell Thermodynamics*; SAND91-0002; Sandia National Laboratory: Albuquerque, NM, 1992.

Appendix. Fragment-Simulating Projectile Deformation

Figure A-1 contains photographs of the sequential stages of fragment-simulating projectile (FSP) deformation during the perforating a 4340 plate. Figure A-2 is the CTH simulation duplicating the conditions of the experimental shot. Figure A-3 is a graphic of the CTH simulation. The thin orange band is ~860 K, the yellow ~650 K, the green ~476 K, and the blue the ambient temperature 300 K. (The ignition temperature of M30 in contact with an 830 gr FSP is 520 K.) The steep temperature gradients between the major temperature zones have not been duplicated in the graphic. The high temperature zones at the impacting edge of the exiting residual FSP are consistent with the premise[1] that most of the mechanical work done in the FSP perforation process is the shearing off of the mushroomed section of the FSP (figure A-1, middle). For a 0° obliquity shot, the chisel point of the FSP acts like a piston and extrudes the metal behind the piston into the mushroom configuration. This movement has been verified by using selected tracer points during the CTH simulations. The hottest regimes, indicating the most mechanical work, will always be at the intersection of the FSP barrel and the impact generated "mushroom" prior to the combined perforation/shearing action.

Figure A-1. Sequential stages of FSP deformation during the perforation of a 4340 plate.

[1]Baker, P. U.S. Army Research Laboratory, Aberdeen Proving Ground, MD. Private communication, 2003.

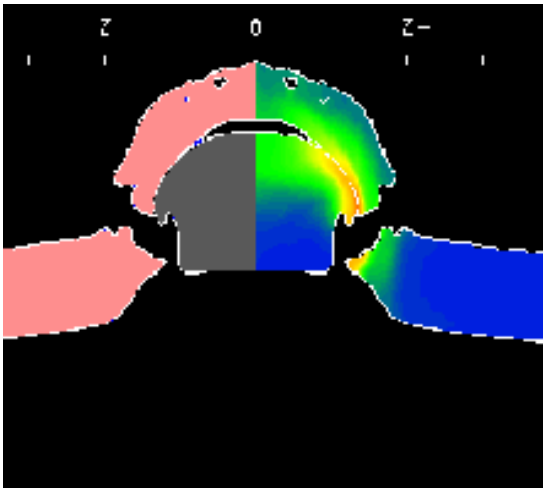

Figure A-2. CTH simulation duplicating the conditions of the experimental shot.

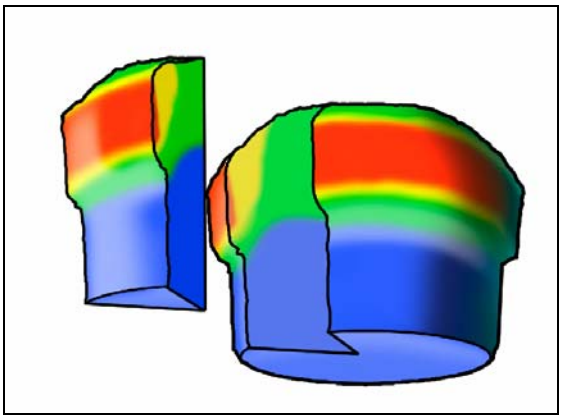

Figure A-3. CTH simulation.

The temperature is a function of the velocity of the FSP and the thickness of the plate. The more resistance to impact, the more deformation and subsequently a larger amount of material sheared off. This results in a higher temperature and larger volume of superheated material. Table 1 shows that the thicker plate and higher perforation velocity gives a lighter weight residual mass.

NO. OF COPIES ORGANIZATION

1 (PDF ONLY) DEFENSE TECHNICAL INFORMATION CTR
DTIC OCA
8725 JOHN J KINGMAN RD
STE 0944
FORT BELVOIR VA 22060-6218

1 US ARMY RSRCH DEV & ENGRG CMD
SYSTEMS OF SYSTEMS INTEGRATION
AMSRD SS T
6000 6TH ST STE 100
FORT BELVOIR VA 22060-5608

1 INST FOR ADVNCD TCHNLGY
THE UNIV OF TEXAS
AT AUSTIN
3925 W BRAKER LN STE 400
AUSTIN TX 78759-5316

1 US MILITARY ACADEMY
MATH SCI CTR EXCELLENCE
MADN MATH
THAYER HALL
WEST POINT NY 10996-1786

1 DIRECTOR
US ARMY RESEARCH LAB
IMNE AD IM DR
2800 POWDER MILL RD
ADELPHI MD 20783-1197

3 DIRECTOR
US ARMY RESEARCH LAB
AMSRD ARL CI OK TL
2800 POWDER MILL RD
ADELPHI MD 20783-1197

3 DIRECTOR
US ARMY RESEARCH LAB
AMSRD ARL CS IS T
2800 POWDER MILL RD
ADELPHI MD 20783-1197

NO. OF COPIES ORGANIZATION

ABERDEEN PROVING GROUND

1 DIR USARL
AMSRD ARL CI OK TP (BLDG 4600)

NO. OF COPIES ORGANIZATION

1 OASD C3I
J BUCHHEISTER
RM 3D174
6000 DEFENSE PENTAGON
WASHINGTON DC 20301-6000

1 OUSD(AT)/S&T AIR WARFARE
R MUTZELBURG
RM 3E139
3090 DEFENSE PENTAGON
WASHINGTON DC 20301-3090

1 OUSD(AT)/S&T LAND WARFARE
A VIILU
RM 3B1060
3090 DEFENSE PENTAGON
WASHINGTON DC 20310-3090

1 UNDER SECY OF THE ARMY
DUSA OR
RM 2E660
102 ARMY PENTAGON
WASHINGTON DC 20310-0102

1 ASST SECY ARMY
ACQSTN LOGISTICS & TECH
SAAL ZP RM 2E661
103 ARMY PENTAGON
WASHINGTON DC 20310-0103

1 ASST SECY ARMY
ACQSTN LOGISTICS & TECH
SAAL ZS RM 3E448
103 ARMY PENTAGON
WASHINGTON DC 20310-0103

1 DIRECTOR FORCE DEV
DAPR FDZ
RM 3A522
460 ARMY PENTAGON
WASHINGTON DC 20310-0460

1 US ARMY TRADOC ANL CTR
ATRC W
A KEINTZ
WSMR NM 88002-5502

1 USARL
AMSRD ARL SL EA
R FLORES
WSMR NM 88002-5513

NO. OF COPIES ORGANIZATION

1 USARL
AMSRD ARL SL EI
J NOWAK
FT MONMOUTH NJ 07703-5601

ABERDEEN PROVING GROUND

1 US ARMY DEV TEST COM
CSTE DTC TT T
APG MD 21005-5055

1 US ARMY EVALUATION CTR
CSTE AEC SVE
R BOWEN
4120 SUSQUEHANNA AVE
APG MD 21005-3013

1 US ARMY EVALUATION CTR
CSTE AEC SVE S
R POLIMADEI
4120 SUSQUEHANNA AVE
APG MD 21005-3013

1 US ARMY EVALUATION CTR
CSTE AEC SV L
R LAUGHMAN
4120 SUSQUEHANNA AVE
APG MD 21005-3013

14 DIR USARL
AMSRD ARL SL
J BEILFUSS
P DEITZ
AMSRD ARL SL B
J FRANZ
M PERRY
P TANENBAUM
AMSRD ARL SL BB
D BELY
D FARENWALD
S JUARASCIO
M RITONDO
AMSRD ARL SL BD
R GROTE
AMSRD ARL SL BE
L ROACH
AMSRD ARL SL E
M STARKS
AMSRD ARL SL EC
J FEENEY
E PANUSKA

NO. OF
COPIES ORGANIZATION

ABERDEEN PROVING GROUND

14 DIR USARL
AMSRD ARL SL BD
M CLARK
J POOLE
D DOMINICK
R KANE
M WARD
AMSRD ARL SL BE
N GERRI (3 CPS)
M MAHAFFEY
P FEDELE
R SAUCIER
AMSRD ARL WM MD
J MONTGOMERY
AMSRD ARL WM TB
P BAKER
L VANDERKIEF

INTENTIONALLY LEFT BLANK.